Thermodynamics and mechanism of the $B1$-$B2$ phase transition in group-I halides and group-II oxides

C. E. Sims, G. D. Barrera,* and N. L. Allan
School of Chemistry, University of Bristol, Cantock's Close, Bristol BS8 1TS, United Kingdom

W. C. Mackrodt
School of Chemistry, University of St. Andrews, St. Andrews, Fife KY16 9ST, Scotland
(Received 21 October 1997)

We study the thermodynamics, mechanism, and kinetic aspects of the $B1$-$B2$ phase transition in alkali halides and alkaline-earth oxides, using both two-body potentials and first-principles periodic Hartree-Fock theory, including *a posteriori* correlation corrections and self-consistent density functional calculations. Both the Buerger and Watanabe-Tokonami-Morimoto mechanisms are shown to be operable, for the activation energies of the two mechanisms are very close. The activation energies predicted by the potential model are always smaller than those from first-principles electronic structure calculations. Transition paths based on both approaches show marked variations with pressure and can be used to rationalize the pressure hysteresis observed experimentally. We discuss the effects of changing cation and anion size and charge on the transition pressures and activation energies and volumes. [S0163-1829(98)11417-0]

I. INTRODUCTION

In recent years, considerable attention has been devoted to understanding the pressure-induced phase transition[1–4] from the Bl (NaCl) to the $B2$ (CsCl) structure, which results in a change in coordination number from 6 to 8. Somewhat surprisingly, however, little attention appears to have been paid to calculations related to kinetic and mechanistic aspects of this transition in these compounds and it is these aspects that are the subject of the current paper. The $B1$-$B2$ transition is of considerable interest as a model for other structural phase transformations, including those of geophysical importance, as it is one of the simplest first-order nondisplacive transitions.

Experimentally, there appear to be large energy barriers to the $B1$-$B2$ transformation. There is evidence that for large, pure crystals the transformation occurs suddenly and simultaneously over the entire crystal volume.[5] To obtain the $B2$ phase the $B1$ crystal must be subjected to a pressure larger than the thermodynamic transition pressure P_{trans}. In the reverse direction a pressure lower than P_{trans} is required. The hysteresis range, defined by the observed pressure difference between the $B1 \rightarrow B2$ and $B2 \rightarrow B1$ transitions, appears to depend on such factors as purity, the thermal and mechanical history of the sample,[6] and the rate of change of applied pressure.[7] The $B2 \rightarrow B1$ transition in CsCl at 718 K and zero pressure has also been investigated by x-ray studies of single crsytals and optical microscopy of single crystals.[8]

The $B1$-$B2$ transformation has been discussed chiefly in the context of two models. The first, which is often the only model presented in standard texts,[9] was proposed initially by Shoji[10] and subsequently modified by Buerger.[11] In common with much of the literature, we refer to this as the Buerger mechanism; it involves a simultaneous increase of the rhombohedral angle of the primitive $B1$ crystallographic cell and a change in the lattice parameter. A second possibility was introduced by Watanabe, Tokonami, and Morimoto[8] (WTM) in their study of the $B2 \rightarrow B1$ transition in CsCl. This mechanism is discussed in more detail in a later section. It involves a concerted translation of adjacent planes relative to one another with simultaneous rearrangements of the ions within each plane.

The choice of theoretical method to address this problem is governed by the essential prerequisite that any such method be capable of accurate prediction of the thermodynamic transition pressure between the two phases. Accordingly, in this paper we present a study of the mechanism and thermodynamics of the $B1$-$B2$ phase transition for series of group-I halides and group-II oxides based on two-body potentials and first-principles Hartree-Fock calculations, with and without *a posteriori* correlation corrections and self-consistent density functional theory (DFT) calculations as implemented in CRYSTAL95.[12,13] Both potential-based and electronic structure methods[3,14–17] have been shown to give thermodynamic transition pressures in good agreement with experiment, not only for $B1$-$B2$, but also for the rutile to fluorite transition.[18]

There has been little previous work on mechanistic aspects of these transitions. Nakagiri and Nomura[19] used a pair potential model to predict a barrier in the WTM mechanism; however, long-range forces were not treated correctly. Later, Ruff *et al.*[20] concluded that the WTM mechanism was favored for RbBr on the basis of isothermal-isobaric molecular dynamics using the well-known Tosi-Fumi potentials.[21] Nga and Ong[22] reported Parrinello-Rahman molecular dynamics using the same potentials, from which they suggested that both the Buerger and WTM mechanisms are essentially equivalent. However, the calculated transition pressures were considerably in excess of the experimentally observed transition pressures (for example, by a factor of 44 in Ref. 20), so that it is unclear whether their conclusions would also apply at lower pressures, closer to the experimental transition

pressures. All these studies used solely two-body empirical potentials. Martín Pendás *et al.*[2] carried out a careful study of the Buerger mechanism in LiCl using an *ab initio* perturbed ion method,[23] while a periodic Hartree-Fock study of the Buerger mechanism in CaO, utilizing pseudopotentials, has been reported by D'Arco *et al.*[24] One of the aims of this paper is to provide a systematic comparison of results obtained using atomistic and *ab initio* techniques and present results for a range of alkali halides and alkaline-earth oxides.

II. THEORETICAL METHODS

A. Atomistic simulations

For the most part, here we have used standard lattice statics methods identical to those employed in earlier studies of halides and oxides and which have been described at length elsewhere.[25] Two-body empirical potentials for MX (M = Li–Rb, X = F–Br) were taken from work by a large number of preivous authors[21,26,27] and, for the alkaline-earth oxides MO (M = Mg–Sr), the consistent set of Buckingham potentials reported by Sangster and Stoneham.[28] Some of these potentials are rigid ion; for those which include the Dick-Overhauser shell model[29] to take some account of the electronic polarization of the lattice, the shell parameters of earlier work were used without alteration. For any structure where ions were not at a center of inversion symmetry (such as those in the WTM mechanism), the energy was minimized with respect to the shell displacements.

To study the effect of temperature, we have calculated free energies using the quasiharmonic approximation[3] in which it is assumed that the Helmholtz free energy A of a crystal at a temperature T can be written as the sum of static and vibrational contributions,

$$A = \Phi_{\mathrm{stat}} + A_{\mathrm{vib}}, \tag{1}$$

where Φ_{stat} is the potential energy of the static lattice. A_{vib} is the vibrational contribution given by the Born expression

$$A_{\mathrm{vib}} = \sum_{\mathbf{q},j} \left(\tfrac{1}{2} h\nu_j(\mathbf{q}) + kT \ln\{1 - \exp[-h\nu_j(\mathbf{q})/kT]\}\right), \tag{2}$$

where the $\nu_j(\mathbf{q})$ are the normal mode frequencies for wave vector $\mathbf{q}$ and k is Boltzmann's constant. The $\nu_j(\mathbf{q})$ are evaluated from the dynamical matrix in the usual way and so are explicit functions of the crystallographic parameters but not of the temperature T. We sum over uniform grids of $\mathbf{q}$ vectors,[30] using successively finer grids until convergence is achieved. None of our potentials gave imaginary frequencies for either crystal structure over the relevant range of volumes considered here. In the static limit, A_{vib} is zero.

For the $B1$ and $B2$ structures the unit cell is described by a single lattice parameter a, so that the equilibrium structure at applied pressure P_{ext} can be found by minimizing the availability[31,32] $\tilde{G} = A + P_{\mathrm{ext}} V$ directly with respect to a. At equilibrium, $P = P_{\mathrm{ext}}$, and the availability equals the Gibbs energy. At the thermodynamic transition pressure P_{trans}, the Gibbs energies of the two phases are equal, but there is a difference in volume, ΔV.

B. *Ab initio* calculations

The all-electron *ab initio* linear combination of atomic orbitals (LCAO) Hartree-Fock (HF) method for periodic systems and its computational implementation in the CRYSTAL computer codes have been described in detail previously.[12,13] The calculations reported here use extended Gaussian basis sets appropriate for the solid state, and these have been taken from previous work on NaF,[15] NaCl,[16] KCl,[33] MgO,[34] and CaO.[35] As in a recent study,[15] the Hay and Wadt small core pseudopotential[36] was used for SrO. Computational cost prevented *ab initio* calculations for the complete set of halides, and some are therefore considered only using two-body potentials. The numerical values of the tolerance parameters involved in the evaluation of the infinite Coulomb and exchange series were identical to those in recent work,[37] and chosen, as previously, to ensure high numerical accuracy. A detailed account for the effect of these tolerances has been given elsewhere.[38] The reciprocal space integration utilized the Monkhorst-Pack sampling scheme[39] with a shrinking factor of 8 and a self-consistent field (SCF) convergence criterion of less than 10^{-3} mHartree. *A posteriori* correlation corrections[40] were based on the correlation-only density functionals of Lee, Yang, and Parr[41] and of Perdew, Becke, and Ernzerhof.[42] We have also carried out SCF DFT calculations, also implemented in CRYSTAL95,[13] based on the Dirac-Slater-LSD (local spin density) exchange potential and the Vosko-Wilk-Nusair parametrization of the Ceperley-Alder free electron gas correlation contribution.[43]

All electronic structure calculations are in the static limit. The electronic energy was determined for a range of volumes for both phases and the corresponding pressure from $-(d\Phi_{\mathrm{stat}}/dV)$, which was evaluated numerically.

III. MECHANISMS

A structural phase transition of a macroscopic crystal involves the movement of a number of atoms of the order of Avogadro's number N_A and, in principle, a potential energy hypersurface of $\sim 3N_A$ dimensions. For the purposes both of defining possible mechanisms, i.e., specific atomic pathways, and their practical calculation, the number of dimensions must clearly be reduced to no more than a few. This is most simply achieved by assuming that some degree of periodicity is retained in the course of the transition, so that the mechanism of the transition can be defined in terms of the size and symmetry of the repeat unit connecting the two phases. The

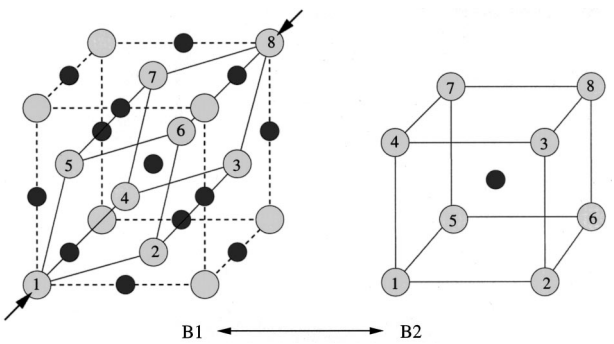

FIG. 1. Buerger mechanism for the conversion of the $B1$ into the $B2$ phase. Primitive unit cells are shown. See also Ref. 45.

retention of periodicity implies that the phase transition is a cooperative process involving a concerted movement of atoms with no account taken of the possible role played by defects. With regard to symmetry, the $B1$-$B2$ transition corresponds to a transition from space group $Fm\bar{3}m$ (no 225) to $Pm\bar{3}m$ (221), which for the primitive unit cells have $R\bar{3}m$ (166) as the highest-symmetry common subgroup, with its subgroups $R3m$ (160), $R32$ (155), $R\bar{3}$ (148), $R3$ (146), $C2/m$ (12), Cm (8), $C2$ (5), $P\bar{1}$ (2), and $P1$ (1) as common subgroups of lower symmetry.[44] Since the repeat unit can be constructed from multiple unit cells ranging from single-unit to $\sim N_A$-unit cells, all possible mechanisms can be defined in terms of the size of the repeat unit and one of the common subgroups which define its symmetry. Thus all mechanisms can be indexed as $M(n,S)$, where n corresponds to the number of atoms in the repeat unit and S the symmetry. It follows that the dimensions of the corresponding potential energy hypersurfaces also depend on the size and symmetry of the repeat unit, varying from two dimensional for two-atom repeat units with $R\bar{3}m$ symmetry to $\sim 3N_A$ dimensional for N_A-atom repeat units with $P1$ symmetry. For any size of repeat unit, the allowable symmetries and variables that define the energy hypersurface can readily be determined. Thus for a two-ion repeat unit, writing the transition in terms of the unit cell variables $(a,b,c,\alpha,\beta,\gamma)$ and irreducible atomic positions $(000;xyz)$,

$B1(Fm\bar{3}m)$				$B2(Pm\bar{3}m)$
$(a_0,a_0,a_0,\pi/3,\pi/3,\pi/3)$		$(a,b,c,\alpha,\beta,\gamma)$		$(b_0,b_0,b_0,\pi/2,\pi/2,\pi/2)$
	$\rightarrow$		$\rightarrow$	
$(000;\frac{1}{2}\frac{1}{2}\frac{1}{2})$		$(000;xyz)$		$(000;\frac{1}{2}\frac{1}{2}\frac{1}{2})$

For example, possible symmetries, intermediate cell variables, and atomic positions are

$$M(2,R\bar{3}m),M(2,R32),M(2,R\bar{3}):\quad (a,a,a,\alpha,\alpha,\alpha)/(000;\tfrac{1}{2}\tfrac{1}{2}\tfrac{1}{2})\quad \text{(two dimensional)},$$

$$M(2,R3m),M(2,R3):\quad (a,a,a,\alpha,\alpha,\alpha)/(000;xxx)\quad \text{(three dimensional)},$$

$$M(2,P\bar{1}),M(2,P1):\quad (a,b,c,\alpha,\beta,\gamma)/(000;\tfrac{1}{2}\tfrac{1}{2}\tfrac{1}{2})\quad \text{(six dimensional)},$$

$$M(2,P1):\quad (a,b,c,\alpha,\beta,\gamma)/(000;xyz)\quad \text{(nine dimensional)}.$$

The Buerger mechanism corresponds to the first of these, namely, $M(2,R\bar{3}m)$, which Martín Pendás *et al.*[2] have shown is the minimum energy path in the full nine-dimensional potential energy surface of $M(2,P1)$. Figure 1 (also see Ref. 45) shows the deformation of the $B1$ cell towards $B2$ in this mechanism.

In general, increasing the size of the repeat unit increases the dimensionality of the hypersurface, so that for four-atom repeat units the intermediate cell variables and atomic positions for the trigonal subgroup transformations and the corresponding symmetries are

$$M(4,R\bar{3}m),M(4,R32),M(4,R\bar{3}):\quad (a,a,a,\alpha,\alpha,\alpha)/(000;\tfrac{1}{2}\tfrac{1}{2}\tfrac{1}{2};\tfrac{1}{4}\tfrac{1}{4}\tfrac{1}{4};-\tfrac{1}{4}-\tfrac{1}{4}-\tfrac{1}{4})\quad \text{(two dimensional)},$$

$$M(4,R\bar{3}m),M(4,R32),M(4,R\bar{3}):\quad (a,a,a,\alpha,\alpha,\alpha)/(000;\tfrac{1}{2}\tfrac{1}{2}\tfrac{1}{2};xxx;-x-x-x)\quad \text{(three dimensional)},$$

$$M(4,R3m),M(4,R3):\quad (a,a,a,\alpha,\alpha,\alpha)/(000;\tfrac{1}{2}\tfrac{1}{2}\tfrac{1}{2},yyy;zzz)\quad \text{(four dimensional)},$$

$$M(4,R3m),M(4,R3):\quad (a,a,a,\alpha,\alpha,\alpha)/(000;xxx;yyy;zzz)\quad \text{(five dimensional)},$$

where $B1$ and $B2$ are $(a_0,a_0,a_0,\pi/3,\pi/3,\pi/3)/(000;\frac{1}{2}\frac{1}{2}\frac{1}{2};\frac{1}{4}\frac{1}{4}\frac{1}{4};-\frac{1}{4}-\frac{1}{4}-\frac{1}{4})$ and $(b_0,b_0,b_0,\pi/2,\pi/2,\pi/2)/(000;\frac{1}{2}\frac{1}{2}\frac{1}{2};\frac{1}{4}\frac{1}{4}\frac{1}{4};-\frac{1}{4}-\frac{1}{4}-\frac{1}{4})$, respectively, and the dimensionality of the Buerger hypersurface is unchanged.

The WTM mechanism corresponds to a four-atom orthorhombic repeat unit which transforms as $Pmm2$ (25), i.e., $M(4,Pmm2)$. The transition can represented as

$B1(Fm\bar{3}m)$				$B2(Pm\bar{3}m)$
$(a_0/\sqrt{2},a_0/\sqrt{2},a_0,\pi/2,\pi/2,\pi/2)$		$(a,b,c,\pi/2,\pi/2,\pi/2)$		$(b_0/\sqrt{2},b_0,b_0,\pi/2,\pi/2,\pi/2)$
$(000;\frac{1}{2}\frac{1}{2}\frac{1}{2})$	$\rightarrow$	$(000;\frac{1}{2}+x\ \frac{1}{2}\frac{1}{2})$	$\rightarrow$	$(000;0\frac{1}{2}\frac{1}{2})$
$(\frac{1}{2}\frac{1}{2}0;00\frac{1}{2})$		$(\frac{1}{2}\frac{1}{2}0;x0\frac{1}{2})$		$(\frac{1}{2}\frac{1}{2}0;\frac{1}{2}0\frac{1}{2})$

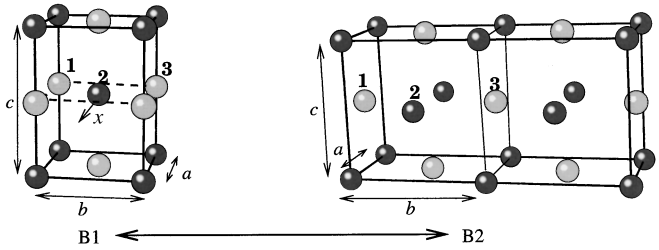

FIG. 2. WTM mechanism for the conversion of the $B1$ into the $B2$ phase. For the $B1$ phase the a- and b-lattice vectors marked lie in the {100} plane of the conventional unit cell.

The WTM mechanism is somewhat more difficult to visualize since it involves both the intralayer rearrangement of ions and the translation of these layers relative to one another. The details are shown in Fig. 2. Referring to the lattice vectors marked in this figure, the $B2$ structure is generated from the $B1$ structure by increasing the b/a ratio from $b=a$ to $b=\sqrt{2}a$. Simultaneously, every alternate (001) plane[46] is displaced by an amount x in the a direction, as depicted also in Fig. 2; x is in units of a. The magnitude of the spacing of the (001) planes, c, also changes. The (001) and $(\bar{1}10)$ planes of the $B1$ structure become, respectively, the (011) and $(0\bar{1}1)$ planes of the $B2$ structure. We have a four-parameter space, denoted here by the magnitudes of the three lattice vectors a, b, and c and x where x is the magnitude of the slip of the (001) planes. Although $\sqrt{2}a=c$ for both $B1$ and $B2$ structures, there is no requirement that this must be obeyed by every point on the minimum-energy pathway. The number of variables is increased further if shell displacements for polarizable anions and cations are also introduced. Calculations involving the WTM mechanism are clearly more costly than those for the Buerger mechanism.

It is straightforward to construct variants of the WTM mechanism with a unit cell involving more than four ions. For example, in adjacent unit cells the relative translation x can be positive or negative. We return briefly to this possibility later, although the cost of generating the required hyperdimensional potential surfaces becomes prohibitive.

IV. RESULTS AND DISCUSSION

A. Energy hypersurfaces: RbBr

We start first with RbBr, in view of the earlier molecular dynamics study of this compound,[20] and calculate the variation of G with P for both the $B1$ and $B2$ phases. Using the same interionic potentials as Ruff *et al.*,[20] the calculated thermodynamic transition pressure P_{trans} for $B1$-$B2$ in the *static* limit is 2.457 GPa. The corresponding value of P_{trans} at 300 K, calculated using quasiharmonic lattice dynamics, is virtually unchanged at 2.464 GPa, showing that vibrational effects are small. These transition pressures are smaller by a factor of 10 than those obtained from an earlier molecular dynamics (MD) study[20] using identical potentials and also in closer agreement with the experimental value of 0.5 GPa.[47]

Turning now to the possible pathways between the $B1$ and $B2$ structures, we have determined the static internal energy (Φ_{stat}) and free energy ($\tilde{G}$) surfaces for the Buerger mechanism. In the static limit, $\tilde{G}=\Phi_{\text{stat}}+P_{\text{ext}}V$. A plot of the $\tilde{G}$ surface as a function of a and α for RbBr with $P_{\text{ext}}=P_{\text{trans}}$ (i.e., with the applied pressure equal to the thermodynamic transition pressure) is given in Fig. 3(a). This shows two minima at the points corresponding to the $B1$ and $B2$ phases. Using standard procedures,[48] it is straightforward to determine the minimum-energy pathway between the two phases, and this is shown in Fig. 3(b), as a function of reaction coordinate s, which we label using the corresponding value of α. There is a clear activation energy barrier of ≈ 5.9 kJ mol^{-1} at this external pressure (P_{trans}). Figure 3(c) indicates the variation of a and α corresponding to the minimum-energy pathways of Fig. 3(b). a decreases as the rhombohedral angle α increases and the cell opens out.

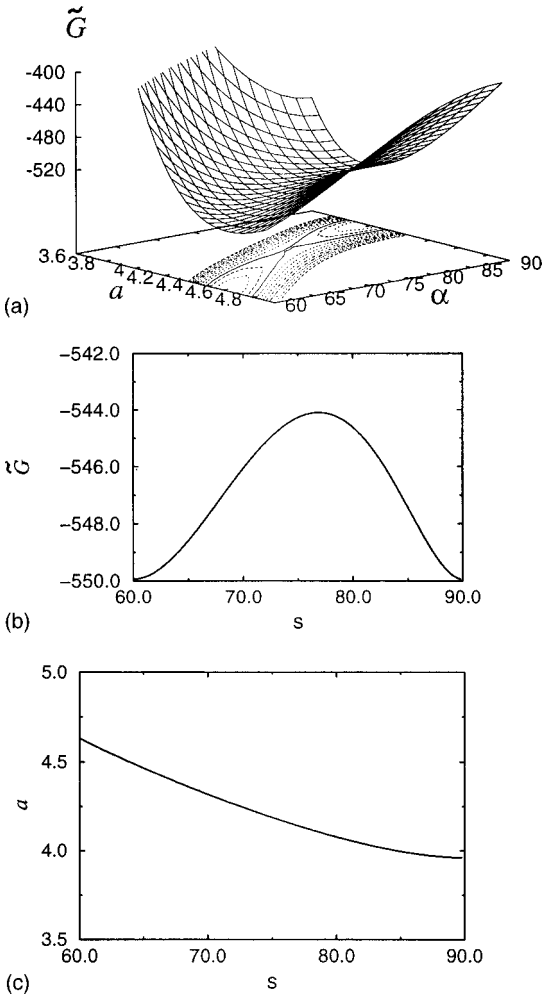

FIG. 3. (a) Free energy surface ($\tilde{G}$), in the static limit, for the Buerger mechanism in RbBr. $P_{\text{ext}}=P_{\text{trans}}$. Energy (kJ mol^{-1}) is plotted as a function of a (Å) and α (deg). (b) Calculated minimum-energy pathway for the Buerger mechanism in RbBr, as a function of reaction coordinate s, which we label using the corresponding value of α. $P_{\text{ext}}=P_{\text{trans}}$. (c) Variation in a (Å) and α (deg) along the pathway in (b).

The analogous plots for the WTM pathway for RbBr, again for $P_{\text{ext}}=P_{\text{trans}}$, are shown in Figs. 4(a)–4(c). Visualization is more complicated here simply because more variables must be considered. a, b, c, and x are as shown in Fig. 2. Each surface in Fig. 4(a) represents the variation of $\tilde{G}$ with

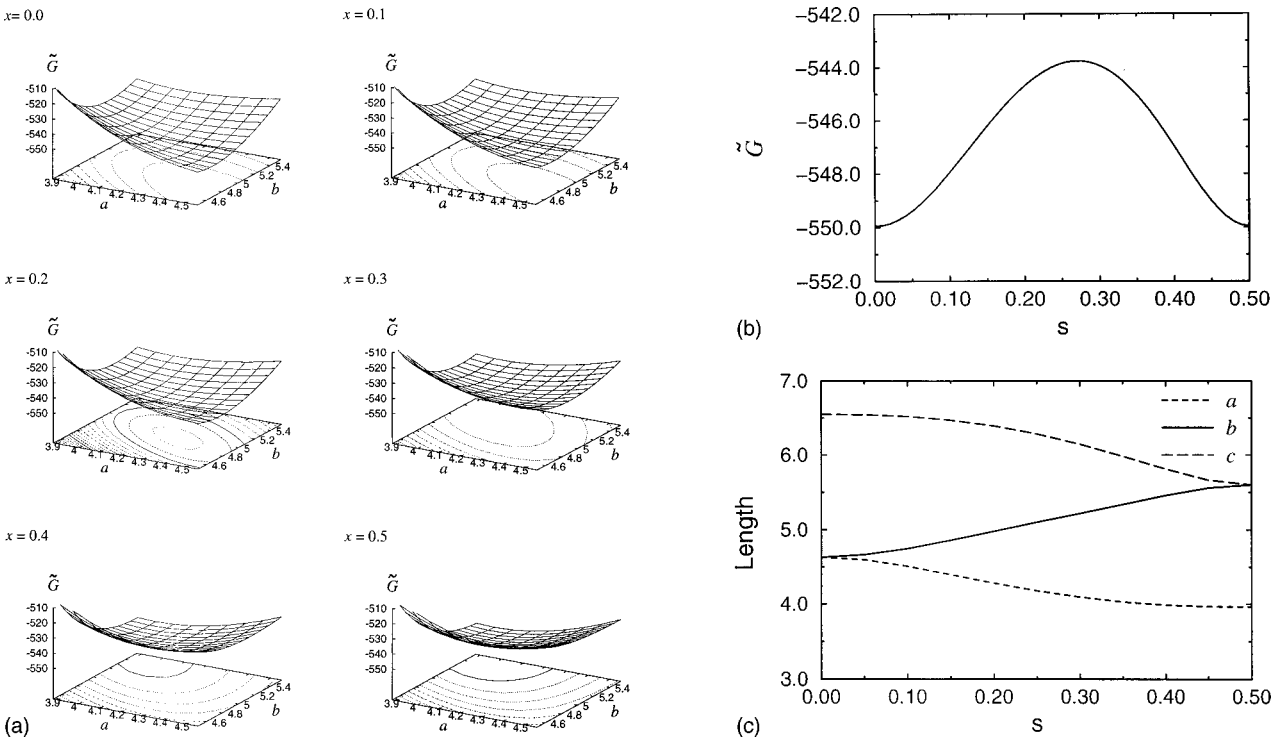

FIG. 4. (a) Free energy surfaces ($\tilde{G}$), in the static limit, for the WTM transition in RbBr. $P_{\text{ext}}=P_{\text{trans}}$. Each surface is plotted at a fixed value of x ($0\leqslant x\leqslant\frac{1}{2}$); for each a, b, and x, $\tilde{G}$ has been minimized with respect to c. a and b are in Å, and energies in kJ mol^{-1}. (b) Calculated minimum energy pathway for the WTM transition in RbBr at the thermodynamic transition pressure as a function of reaction coordinate s, which we label using the corresponding value of x. (c) Variations in the lattice parameters a, b, and c (Å) (as defined in Fig. 2) along the pathway in (b).

the lattice parameters a and b for fixed x; at each point (a,b), the energy has been optimized with respect to c. The computed minimum-energy pathway is shown in Fig. 4(b) and the corresponding variation of the lattice parameters given in Fig. 4(c). The latter shows that, although $c/a=\sqrt{2}$ at the end points of the transition, the ratio is not constant during the transition. The minimum-energy pathway in Fig. 4(b) indicates that, just as for the Buerger mechanism, the WTM mechanism is also an activated process, with a similar barrier of $\sim$6.2 kJ mol^{-1}. A WTM-like mechanism based on a larger repeat unit of eight ions has a slightly smaller activation energy barrier, $\sim$6.0 kJ mol^{-1}, than that for the minimum possible periodic cell, but still comparable to that for the Buerger mechanism. In this context it is worth recalling the earlier MD studies of this transition in RbBr (Ref. 20) based on identical potentials to those used in this work. These studies found a WTM mechanism, but only at a pressure far above the observed transition pressure, so that it is unclear as to whether the same mechanism would operate at pressures much closer to the observed transition pressure.

In view of the experimental observations of hysteresis in the applied pressure, we have calculated Φ_{stat} and $\tilde{G}$ surfaces at applied pressures both higher than and lower than P_{trans}. At zero applied pressure, of course, the Φ_{stat} and $\tilde{G}$ surfaces are identical. As the pressure increases, the difference in Gibbs energy between the $B1$ and $B2$ phases decreases.

Figure 5 shows the calculated minimum-energy pathways for the $B1$-$B2$ transition in RbBr at a range of applied pressures for the Buerger mechanism. At *all* these pressures the activation energies for the Buerger and WTM mechanisms are very close, with those for $B1\rightarrow B2$ and $B2\rightarrow B1$ different at all pressures except P_{trans}. The $B1\rightarrow B2$ activation energy decreases exponentially with increasing pressure, whereas the $B2\rightarrow B1$ activation energy increases. At room temperature thermal contributions to the free energy are not large enough to overcome the energy barrier. Pressures with thermally accessible barriers for the $B1\rightarrow B2$ transition are larger than the thermodynamic transition pressures. For $B2\rightarrow B1$, pressures with accessible barriers are smaller than P_{trans}. Consider a sample with the $B1$ structure. On com-

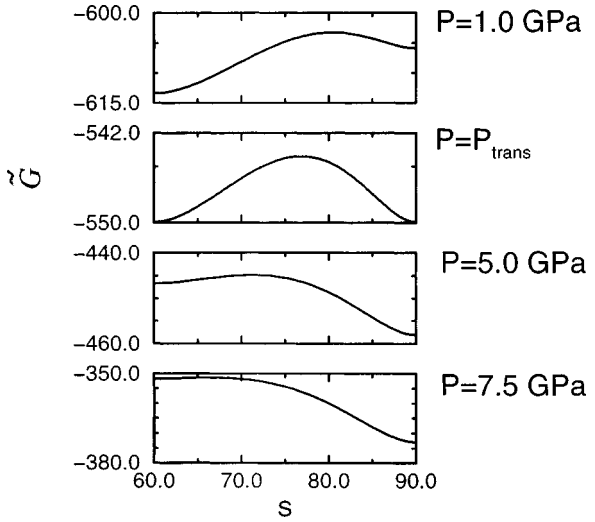

FIG. 5. Free energy $\tilde{G}$ (kJ mol^{-1}) vs s (deg) at a range of applied pressures P for the Buerger mechanism in RbBr.

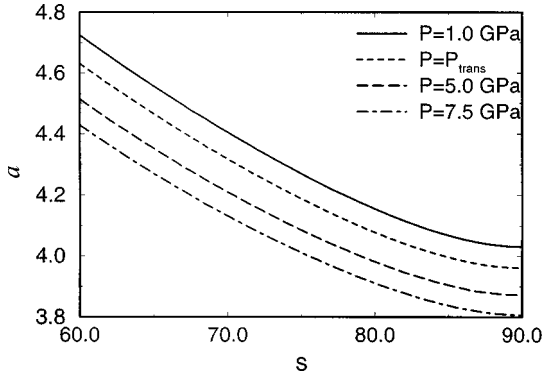

FIG. 6. a (Å) vs s (deg) at a range of applied pressures P for the Buerger mechanism in RbBr.

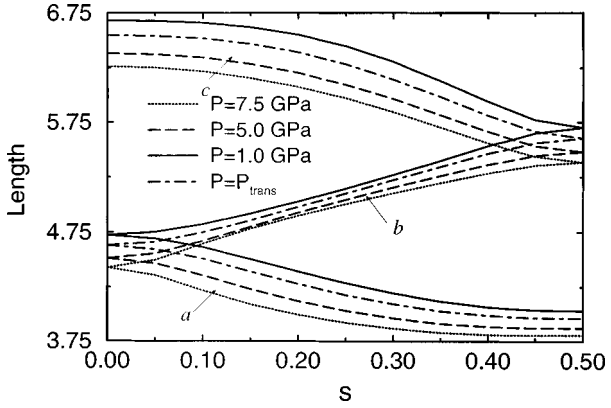

FIG. 7. Lattice parameters a, b, and c (Å), as defined in Fig. 2, vs s at a range of applied pressures P for the WTM mechanism in RbBr.

pression, the transition to the $B2$ phase takes place at a pressure considerably in excess of the thermodynamic transition pressure. Once the $B2$ structure has formed, then on lowering the pressure the reverse transformation occurs only at a pressure much lower than P_{trans}.

We have also investigated the variation of the unit cell geometry along the minimum-energy pathways as a function of pressure. For the Buerger mechanism curves of a vs α at different pressures are virtually parallel (Fig. 6). Martín Pendás *et al.*[2] have discussed how the form of this plot is largely determined by symmetry considerations. Similarly for the WTM mechanism (Fig. 7), the variations in the three lattice parameters at different pressures lie almost parallel to each other.

B. Energy hypersurfaces: Halides and oxides

We now consider a wider range of halide and oxide systems, the hypersurfaces of which we have examined in somewhat less detail. The Buerger and WTM mechanisms were

TABLE I. Calculated (simulation and *ab initio*) and experimental thermodynamic transition pressures (GPa) between the $B1$ and $B2$ phases for the halides and oxides studied. In the case of the simulations, transition pressures in the static limit are listed as well as transition pressures at 300 K, calculated using quasiharmonic lattice dynamics.

	Calculated transition pressure (GPa)					
	Static	Quasiharmonic ($T=300$ K)	*Ab initio* HF	HF +*a posteriori* correlation correction	DFT	Experiment
LiCl	185	181				N/A
NaF	19.6	19.2	32.6	25.0 [a]		23±3 [b]
NaCl	34.1	33.3	38.3	35.9 [a] 27.7[d]	24.6	27 [c]
KCl	4.0	3.9	4.45	2.0		2.0 [e]
RbBr	2.5	2.5				0.5 [f]
MgO	151	156	>240		237	>227 [g]
CaO	93.7	93.4	70.4	61.8 [a] 54.8[d]	53.5 [h]	60 [i]
SrO	81.8	81.6	41.8	28.6 [a]	31.7	36±4[j]

[a]Perdew-Burke-Ernzerhof functional (Ref. 42).
[b]Reference 50.
[c]Reference 51.
[d]Lee-Yang-Parr functional (Ref. 41).
[e]Reference 52.
[f]Reference 47.
[g]Reference 53.
[h]For comparison, a value of 58 GPa has recently been found with the first-principles pseudopotential method within the local density approximation (Ref. 54).
[i]Reference 55.
[j]Reference 56.

TABLE II. Calculated activation energies (kJ mol^{-1}) at the appropriate thermodynamic transition pressure (P_{trans}), for the Buerger and WTM mechanisms, from atomistic simulation, periodic Hartree-Fock calculations and periodic Hartree-Fock calculations including *a posteriori* correlation corrections.

	Buerger mechanism				WTM mechanism
	Atomistic simulation	*Ab initio*			Atomistic simulation
		HF	HF +*a posteriori* correlation [a]	DFT	
LiCl	20				21
NaF	7.3	16	16		7.8
NaCl	9.8	38	33	33	10
KCl	7.1				7.0
RbBr	5.9				6.2
MgO	22				24
CaO	20	62	62	51	22
SrO	17	30	31	29	20

[a]Perdew-Burke-Ernzerhof functional (Ref. 42).

studied for all systems using two-body potentials. In addition, our available computational resources permitted a study of the Buerger mechanism in NaF, NaCl, CaO, and SrO using periodic Hartree-Fock calculations, including *a posteriori* correlation corrections, in the static limit, and SCF DFT calculations for NaCl, CaO, and SrO.

Table I lists the calculated thermodynamic transition pressures. A comparison between the *ab initio* values and the experimental pressures (also listed) shows that agreement between the two is very good for all the compounds. The Hartree-Fock transition pressures are all slightly larger than experiment and are reduced with the inclusion of *a posteriori* correlation corrections. The static transition pressures calculated using the potential-based approach are in good agreement with experiment for the halides. The agreement is poorer for CaO and SrO, but for consistency we have included results for the entire set of potentials from Ref. 28.

Also given in Table I are transition pressures calculated using lattice statics and quasiharmonic lattice dynamics for a temperature of 300 K. As for RbBr, the differences between these transition pressures and those for the static limit are very small, which again suggests that vibrational effects are relatively unimportant.

The results for the activation energy (E_a) barriers at the thermodynamic transition pressure, calculated as before for RbBr, are summarized in Table II. Turning first to the results obtained using pair potentials, the barriers for the Buerger and WTM mechanisms are close for all systems. The differences between the two activation energies are of the same order as the thermal contributions to the free energies. In general, activation energies for oxides are larger than those for halides, so that as noted previously, halides may not always serve as useful model systems for oxides[2] at high pressures. Table II also indicates that for a given anion, the activation energy decreases with increasing cation size. For the halides it appears that E_a decreases as the ratio of the ionic radii r_+/r_- increases.

Activation volumes, given by the difference between the volume of the transition state and that of the equilibrium $B1$ structure, at the transition pressure, calculated for the Buerger mechanism using atomistic simulation, are listed in Table III. Large activation volumes are associated with small thermodynamic transition pressures. Transition states appear to occur further along the reaction coordinate for oxides than for halides and occur later on descending a group.

Where we have been able to carry out periodic Hartree-Fock calculations (Table II), the conclusions are qualitatively similar to those from potential-based simulations. The inclusion of *a posteriori* correlation corrections leaves the barrier heights virtually unchanged; furthermore, the SCF DFT barrier heights for NaCl, CaO, and SrO are only slightly smaller than the HF value. The *ab initio* activation energies are all larger than the simulation values by at least a factor of ≈ 2. Possible reasons for this include the failure of the two-body potential model in the simulations to describe correctly the energetics of the unusual coordination of the transition state and possible effects due to basis set superposition error in the *ab initio* calculations.

For each system, we have investigated the change in activation energy with pressure, and from these the resulting hysteresis cycle can readily be understood, as in the case of RbBr. While experiments indicate the presence of a pressure hysteresis, there is insufficient data for even a qualitative comparison at this stage. The overall kinetics of a solid-state reaction depends on the nucleation and growth mechanisms, which involve additional energy terms such as the interfacial energy, which has not been considered here. This, and the neglect of defects, rule out the possibility of a meaningful quantitative comparison. Moreover, preliminary estimates[49] based on standard nucleation theory indicate that the hysteresis range for oxides is larger than that for halides. Estimated half-lives appear to be very dependent on pressure and can vary by over 10^6 over less than 1 GPa; hence, transitions in both forward and backward directions are predicted to take

TABLE III. Calculated volumes of activation (10^{-7} m^3 mol^{-1}) at the appropriate thermodynamic transition pressure (P_{trans}), for the Buerger mechanisms, from atomistic simulation.

LiCl	NaF	NaCl	KCl	RbBr	MgO	CaO	SrO
−2.3	−5.5	−4.7	−17.1	−23.3	−3.1	−4.7	−5.2

place over a narrow pressure range. In addition, the hysteresis range decreases markedly with temperatures, suggesting that high-temperature experiments are required to obtain reliable equilibrium data.

V. CONCLUSIONS

In this paper we have studied possible mechanisms for the $B1$-$B2$ phase transition in alkali halides and alkaline-earth oxides, using both potential-based and first-principles periodic Hartree-Fock calculations, including *a posteriori* correlation corrections and self-consistent density functional calculations. Barriers have been estimated which suggest that the Buerger and the Watanabe-Tokonami-Morimoto mechanisms have very similar activation energies. It has also been possible to rationalize the observed pressure hysteresis in these systems. There are clear trends down a given group of the Periodic Table and between halides and oxides. The results obtained from *ab initio* theory parallel those obtained from the atomistic simulation model, although the *ab initio* barrier heights are in excess of the pair-potential values. Our results are sufficiently encouraging for us to consider mechanisms in more complex systems in future work, as well as the use of more sophisticated methods for the estimation of the rates of transition.

ACKNOWLEDGMENTS

This work was supported by EPSRC Grant Nos. GR/K05979 and GR/L31340. C.E.S. wishes to thank EPSRC and ICI Explosives for support. G.D.B. gratefully acknowledges financial support from la Universidad de Buenos Aires. His contribution to this work was made possible by means of a grant from el Consejo Nacional de Investigaciones Científicas y Técnicas de la República Argentina.

*Permanent address: Universidad de Buenos Aires, Facultad de Ciencias Exactas y Naturales, Departamento de Química Inorgánica, Analítica y Química Física, Pabellón 2, Ciudad Universitaria, 1428 Buenos Aires, Argentina.

[1] For example, P.W. Bridgman, *The Physics of High Pressure* (Dover, New York, 1970).

[2] A. Martín Pendás, V. Luaña, J.M. Recio, M. Flórez, E. Francisco, M.A. Blanco, and L.N. Kantorovich, Phys. Rev. B **49**, 3066 (1994).

[3] N.L. Allan, M. Braithwaite, D.L. Cooper, W.C. Mackrodt, and B. Petch, J. Chem. Soc., Faraday Trans. **89**, 4369 (1993), and references therein.

[4] For example, B.B. Karki, L. Stixrude, S.J. Clark, M.C. Warren, G.J. Ackland, and J. Crain, Am. Mineral. **82**, 51 (1997).

[5] For example, O. Blaschko, G. Ernst, G. Quittner, G. Pépy, and M. Roth, Phys. Rev. B **36**, 474 (1987).

[6] A. Lacam and J. Peyronneau, J. Phys. (Paris) **34**, 1047 (1973).

[7] X. Li and R. Jeanloz, Phys. Rev. B **36**, 474 (1987).

[8] M. Watanabe, M. Tokonami, and N. Morimoto, Acta Crystallogr., Sect. A: Cryst. Phys., Diffr., Theor. Gen. Crystallogr. **33**, 294 (1977).

[9] For example, A.R. West, *Solid State Chemistry and Its Applications* (Wiley, New York, 1984).

[10] H. Shoji, Z. Kristallogr. **77**, 381 (1931).

[11] J. Buerger, in *Phase Transformation in Solids*, edited by R. Smoluchowski, J.E. Mayers, and W.A. Weyl (Wiley, New York, 1951).

[12] C. Pisani, R. Dovesi, and C. Roetti, *Hartree-Fock Ab Initio Treatment of Crystalline Systems* (Springer-Verlag, Berlin, 1988).

[13] R. Dovesi, V.R. Saunders, C. Roetti, M. Causa, N.M. Harrison, R. Orlando, and E. Aprà, *CRYSTAL 95, User Manual* (Università di Torino and CCLRC Daresbury Laboratory, Daresbury, 1996).

[14] N.L. Allan, and M. Braithwaite, D.L. Cooper, W.C. Mackrodt, and B. Petch, Mol. Simul. **9**, 161 (1992).

[15] A. Zupan, I. Petek, M. Causà, and R. Dovesi, Phys. Rev. B **48**, 799 (1993).

[16] E. Aprà, M. Causà, M. Prencipe, R. Dovesi, and V.R. Saunders, J. Phys.: Condens. Matter **5**, 2969 (1993).

[17] R.L. Erikson, E. Eary, and C.J. Hostetler, J. Chem. Phys. **99**, 336 (1993).

[18] N.L. Allan, R.I. Hines, W. C. Mackrodt, and M.D. Towler, J. Chem. Phys. **100**, 4710 (1994): G.D. Barrera, M.B. Taylor, N.L. Allan, T.H.K. Barron, L.N. Kantorovich, and W.C. Mackrodt, *ibid.* **107**, 4337 (1997).

[19] N. Nakagiri and M. Nomura, J. Phys. Soc. Jpn. **51**, 2412 (1982).

[20] I. Ruff, A. Baranyai, E. Spohr, and K. Heinzinger, J. Chem. Phys. **91**, 3148 (1989).

[21] M.P. Tosi and F.G. Fumi, J. Phys. Chem. Solids **25**, 31 (1964).

[22] Y.A. Nga and C.K. Ong, Phys. Rev. B **46**, 10 547 (1992).

[23] V. Luaña and L. Pueyo, Phys. Rev. B **41**, 3800 (1990).

[24] P. D'Arco, L. Jolly, and B. Silvi, Phys. Earth Planet. Inter. **72**, 286 (1992).

[25] See, for example, *Computer Simulation of Solids*, editd by C.R.A. Catlow and W.C. Mackrodt (Springer-Verlag, Berlin, 1982).

[26] M.J.L. Sangster and R.M. Atwood, J. Phys. C **11**, 1541 (1978).

[27] C.R.A. Catlow, K.M. Diller, and M.J. Norgett, J. Phys. C **12**, 451 (1979).

[28] M.J.L. Sangster and A.M. Stoneham, Philos. Mag. B **52**, 717 (1985).

[29] B.G. Dick and A. W. Overhauser, Phys. Rev. **112**, 90 (1958).

[30] D.J. Chadi and M.L. Cohen, Phys. Rev. B **8**, 5747 (1973).

[31] A.B. Pippard, *The Elements of Classical Thermodynamics* (Cambridge University Press, Cambridge, England, 1964).

[32] M.B. Taylor, G.D. Barrera, N.L. Allan, and T.H.K. Barron, Phys. Rev. B **56**, 14 380 (1997).

[33] R. Dovesi, C. Roetti, C. Freyria-Fava, E. Aprà, V.R. Saunders, and N.M. Harrison, Philos. Trans. R. Soc. London, Ser. A **341**, 203 (1992).

[34] M.I. McCarthy and N.M. Harrison, Phys. Rev. B **49**, 8574 (1994).

[35] W.C. Mackrodt, N.M. Harrison, V.R. Saunders, N.L. Allan, M.D. Towler, E. Aprà, and R. Dovesi, Philos. Mag. A **68**, 653 (1993).

[36] P.J. Hay and W.R. Wadt, J. Chem. Phys. **82**, 270 (1985).

[37] M.D. Towler, N.L. Allan, N.M. Harrison, V.R. Saunders, W.C. Mackrodt, and E. Aprà, Phys. Rev. B **50**, 5041 (1994).

[38] R. Dovesi, M. Causà, R. Orlando, C. Roetti, and V.R. Saunders, J. Chem. Phys. **92**, 7402 (1990).

[39] H.J. Monkhorst and J.D. Pack, Phys. Rev. B **13**, 5188 (1976).

[40] For examples, see M. Causà and A. Zupan, Chem. Phys. Lett. **220**, 145 (1994); Int. J. Quantum Chem. **S28**, 633 (1995).

[41] C. Lee, W. Yang, and R.G. Parr, Phys. Rev. B **37**, 785 (1988).

[42] J.P. Perdew, K. Burke, and M. Ernzerhof, Phys. Rev. Lett. **77**, 3865 (1996).
[43] S.H. Vosko, L. Wilk, and M. Nusair, Can. J. Phys. **58**, 1200 (1980).
[44] *International Tables for Crystallography*, edited by T. Hahn (Reidel, Dordrecht, 1983).
[45] See the world wide web http://dougal.chm.bris.ac.uk/~allan
[46] The label (001) refers to the $B1$ structure throughout.
[47] G.H. Shaw, J. Geophys. Res. **79**, 2635 (1974).
[48] W.H. Press, S.A. Teukolsky, W.T. Vettering, and B.P. Flannery, *Numerical Recipes in Fortran: The Art of Scientific Computing*, 2nd ed. (Cambridge University Press, Cambridge, England, 1992).
[49] C.E. Sims and N.L. Allan (unpublished).
[50] Y. Sato-Sorensen, J. Geophys. Res. **88**, 3543 (1983).
[51] S. Froyen and M.L. Cohen, J. Phys. C **19**, 2623 (1986).
[52] S.N. Vaidya and G.C. Kennedy, J. Phys. Chem. Solids **32**, 951 (1971).
[53] T.H. Duffy and T.J. Ahrens, J. Geophys. Res. **100**, 529 (1995).
[54] B.B. Karki, G.J. Ackland, and J. Crain, J. Phys.: Condens. Matter **9**, 8579 (1997).
[55] P. Richet, H.K. Mao, and P.M. Bell, J. Geophys. Res. **93**, 15 279 (1986).
[56] Y. Sato and R. Jeanloz, J. Geophys. Res. **86**, 1773 (1981).